Predicting the Load-Carrying Capacity of Reinforced Concrete Structural Element

HOKEŠ FILIP, MARTIN HUŠEK, JIŘÍ KALA, PETR KRÁL
Faculty of Civil Engineering, Institute of Structural Mechanics
Brno University of Technology
Veveří 331/95, 602 00 Brno
CZECH REPUBLIC
hokes.f@fce.vutbr.cz, husek.m@fce.vutbr.cz, kala.j@fce.vutbr.cz, kral.p@fce.vutbr.cz,
http://www.fce.vutbr.cz

Abstract: - The load-carrying capacity of structural elements manufactured from concrete or reinforced concrete can be determined via classic approaches formulated within the statics of structures and linear theory of elasticity. These methods, despite being incorporated in relevant regulations, can nevertheless suffer from reduced effectivity of the final design. In this context, more realistic prediction of the load-carrying capacity of structural elements is achievable via utilizing the nonlinear constitutive law in the numerical computation. Using a nonlinear material model to simulate the behavior of concrete structures is, however, confronted with the problem that consists in the set of unknown parameters related to the selected constitutive law. These parameters can be mechanico-physical or fracture-mechanical, and their values are eventually obtainable by applying inverse analysis methods to the experimentally measured data. One of these techniques is based on exploiting an optimization algorithm, which enables us to minimize the difference between the measured and computed load-displacement curves. The present paper characterizes the inverse identification of material parameters in relation to the Menétrey-Willam material model used in the performed fracture test and discusses the subsequent computation of the load-carrying capacity of a reinforced concrete element executed via the same material model.

Key-Words: - Concrete, reinforced concrete, nonlinear material model, fracture mechanics, fracture test, optimization, inverse identification.

1 Introduction

The process of designing a building structure invariably requires the satisfaction of major criteria, including the primary factors of load-carrying capacity and usability. The actual compliance with the contents of such criteria is then embodied in the provisions of relevant standards and regulations. At present, these documents mostly exploit the methodologies of limit states and partial reliability coefficients [1], whose consistent application ensures the necessary safety, usability, and long life. The designing of concrete and reinforced concrete building structures is governed by the standard EN 1992-1-1 [2], which nevertheless utilizes the assumptions of linear elasticity theory and thus may introduce a certain degree of inefficiency into any structural computation cycle that merely relies on rigorous application of the provisions. Considering the potential of current information technologies, and in view of the results achieved within theoretical research into nonlinear material models of concrete, we can claim that the use of novel constitutive relations is a precondition leading us towards even more optimal structural design.

Within nonlinear material models of concrete, it is presently possible to identify several branches of development. One of such branches exploits the postulates of linear and nonlinear fracture mechanics, described in detail by the authors of reference [3], and is aptly complemented with another category, which has grown upon the assumptions of plasticity theory. A well-conceived historical survey of the material models is proposed within relevant papers by Cicekli et al. [4] and Grassl et al., [5]; both these articles, however, also suggest that using simple plasticity theory to describe the behavior of concrete and reinforced concrete structures does not constitute a satisfactory procedure, mainly due to the decreasing material stiffness caused by the formation and expansion of cracks. This view then inspired the generation of yet another significant branch, namely, one referred to as damage theory. The results obtained from the research in this field nevertheless indicate that the use of the theory as a sole tool is

again not entirely optimal, primarily owing to the inability of the derived material models to capture emerging irreversible deformations and inelastic volume changes of concrete [5]. In the context of developmental categories within the modeling of nonlinear behavior in concrete, we can point further to the DEM (discrete element method) [6] and SPH methods [7,8,9] and the widely favored XFEM (extended finite element method) [10]. The above-mentioned drawbacks of inherent with some of the theories are suitably eliminated via combining the tools into a single concept, observing their mutual complementarity. Currently, we can thus utilize material models of concrete which join together plasticity and damage theories or combine plasticity theory with the theoretical fundamentals of nonlinear fracture mechanics. An example of the latter approach consists in multiPlas, a database of elasto-plastic material models [11] to facilitate nonlinear material computation via the finite element method in ANSYS [12].

The correct application of the discussed models rests upon a relatively broad set of mechanico-physical and fracture-mechanical input parameters of the given constitutive relations. In a substantial number of cases, the values of such parameters are not known in advance; however, the problem can be solved through a simple fracture experiment with subsequent inverse identification of the parameters from the measured data. Within inverse identification, we can employ methods exploiting the training of artificial neural networks [13] or, alternatively, an optimization algorithm [14]. The inverse identification procedure with optimization is based on the effort to reduce the difference between a measured loading curve and one produced by the numerical simulation of a fracture test performed on a computing system [15,16]

Considering the above facts, we drafted a paper to estimate the load-carrying capacity of a reinforced concrete element by means of nonlinear numerical simulation in ANSYS. The actual process involved the application of the Menétrey-Willam material model from the multiPlas database, with the correct setting of the model performed using the inverse identification of its input parameters via a genetic optimization algorithm implemented in the ANSYS Workbench environment. The present article thus proposes a comprehensive description of the entire procedure, including the characterization of the input data, fracture experiment, computational and material models, inverse identification and nonlinear numerical simulation aimed to predict the load-carrying capacity of the selected reinforced concrete element. The paper also constitutes a part of the effort to find the maximal force to be exerted, employing a test device for the experimental verification of the results; such an apparatus will be designed by the author within the future research phases.

For easier orientation within the text, the contribution is divided into chapters which are going to explain the steps of the procedure of predicting the load-carrying capacity of the reinforced concrete beam. The second chapter is devoted to formulation of the solved problem and description of fracture experiment, which was used for identification of material parameters needed for simulation of reinforced beam. The third chapter describes the process of the inverse identification where material and computational model utilized for simulation of fracture experiment is presented in detail. This chapter also brings description of the improved sensitivity analysis. The fourth chapter finally deals with the simulation of the reinforced beam with use of identified material parameters and brings prediction of the load-carrying capacity of this beam. The last chapter of the paper describes conclusions.

2 Problem Formulation

The presented paper is primarily aimed to analyze the load-carrying capacity of a reinforced concrete element and to characterize the behavior of the given structure during loading. In this context, the central purpose consists in obtaining the diagram of load L and displacement d, which is to be verified via experimental testing of a real sample. The general task, however, is rendered problematic by unknown input characteristics of the applied material; in view of the fact, the prediction analysis of the load-carrying capacity of a reinforced concrete element was subdivided into two main phases outlined below.

Within the first stage, we solved the inverse identification of the mechanico-physical and fracture-mechanical parameters of the material model of concrete used to simulate the actual reinforced concrete structure. The second phase then already comprised the numerical simulation of the behavior of the structure, whose parameters had been identified.

2.1 Fracture Experiment

To identify the parameters of the material model, we used the L-d curve measured in the course of the experiment described in [17].

The sample tested by the authors of [17] was a 28 day old concrete beam manufactured from class

C20/25 concrete and exhibiting the slump value of F45. The dimensions of the beam corresponded to 360 x 120 x 58 mm, and the notch height equaled 40 mm. The beam was subjected to a three point bending test, with the distance between the supports set to be 300 mm. The fracture experiment is schematically shown in Fig. 1.

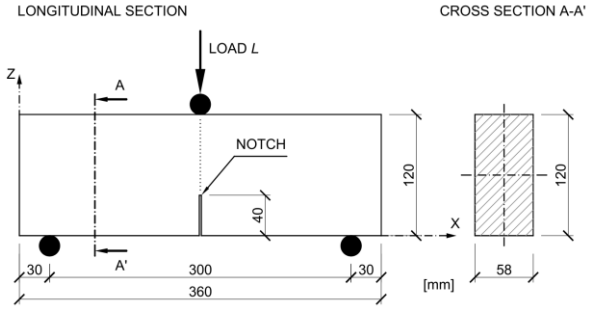

Fig. 1. Idealization of the testing configuration

2.2 Reinforced Concrete Element

For the analysis of the load-carrying capacity, with respect to the good availability and low cost of the test sample, we selected a window lintel having the length of 1190 mm, height cross section of 140 mm, and width of 100 mm. In the lintel, the use of the same type of concrete as that applied previously in the fracture test samples was assumed; however, due to the unavailable product documentation related to the given lintel, we considered the preliminary, informative character of the calculation to assume only the version with a reinforcing bar of Φ8 mm class B500B at the lower face of the element.

Similarly to the sample in the fracture experiment, the analyzed element was exposed to three-point bend loading with the distance of 1 m between the supports. The relevant configuration is schematically represented in Fig. 2.

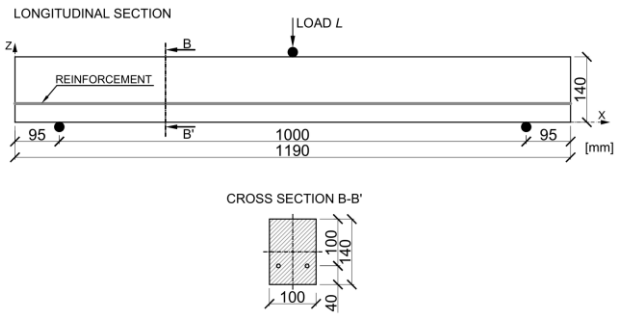

Fig. 2. Idealization of the tested reinforced beam

3 Inverse Identification of Material Model Parameters

The inverse identification of parameters of the Menétrey-Willam material model selected from the multiPlas database was performed using a MOGA genetic algorithm within ANSYS Workbench. Considering the repeated computation, the creation of the computational model, setting of the material one, and formation of the resulting *L-d* curve were all controlled via a pre-programmed batch in the classic environment of ANSYS 15.0.

3.1 Computational Model

The geometry of the computational model of the test sample was, in all of the above-mentioned dimensions, covered with a regular mesh of planar finite elements (PLANE182) exhibiting the edge length of 6 mm. The task was solved as a plane stress problem, with the thickness of 58 mm assigned to all elements of the model. As already noted, the task had been simplified from a 3D problem to a 2D plane stress one in order to reduce the computational time to a single numerical simulation. The notch in the test sample was modeled using two lines having a common node at the top of the notch. At the location of the supports, zero deformations were prescribed in the direction of the vertical axis *z*, and, to ensure the solvability of the task, horizontal deformation was prevented at the position of the introduced load. The load in the model had been entered as vertical deformation d_{max} exhibiting the magnitude of 0.0007 m. In the computational model of the test sample, we also pursued certain simplification within the region above the supports, where, unlike the other portions of the computational model, the elements were assigned a linearly elastic material. This correction was carried out with respect to the occurrence of local stress peaks at the location of the boundary conditions; this action, however, did not affect the accuracy of the results, because the area of interest with nonlinear behavior was positioned above the top of the notch.

3.1 Material Model

The applied material model, Menétrey-Willam, belongs to the group of nonlinear material models of concrete, namely, to a set of tools which cannot capture the effect exerted by the rate of deformation on the stress. As such, the model was suitable for the numerical simulation of the three-point bending test on a notched concrete beam. In these models, irreversible deformations occur when the preset criterion is achieved, and the total deformation vector

$\boldsymbol{\varepsilon_{tot}}$ is assumed to decompose into an elastic $\boldsymbol{\varepsilon_{el}}$ and a plastic $\boldsymbol{\varepsilon_{pl}}$ part [18].

The criterion of the generation of plastic deformations is given by the prescribed yield surface function. The selected material model, Menétrey-Willam [19], exploits the Willam-Warnke yield surface [20], which, unlike the Drucker-Prager one, embodies the function of not only the first and the second but also the third invariant of the deviatoric stress tensor (referred to as lode angle). Such adjustment enables us to refine the angles of the deviatoric sections of the yield surface, whose distance from the hydrostatic axis in Haigh–Westergaard stress space is moreover not constant.

From the perspective of using the FEM, the selected material model utilizes the smeared cracks approach [21]. Further, the given problem was solved employing the version with the softening function based on the dissipation of the specific fracture energy G_f, which thus acts as one of the parameters being sought. With respect to the need of eliminating the negative dependence of the solution on the size of the finite element mesh, the Menétrey-Willam nonlinear model uses Bazant's crack band concept [22]. To facilitate the corresponding nonlinear operation of the model, we had to predefine 12 parameters in total; these are briefly characterized in Table 1 below.

Table 1. A brief definition of the Menétrey-Willam material model parameters

Par.	Unit	Description
E	[Pa]	Young's modulus of elasticity
ν	[-]	Poisson's ratio
f_c	[Pa]	Uniaxial compression strength
f_t	[Pa]	Uniaxial tension strength
k	[-]	Ratio between biaxial compressive strength and uniaxial compressive strength
ψ	[°]	Dilatancy angle (friction angle)
ε_{ml}	[-]	Plastic strain corresponding to the maximum load
G_{fc}	[Nm/m^2]	Specific fracture energy in compression
Ω_{ci}	[-]	Relative stress level at the start of nonlinear hardening in compression
Ω_{cr}	[-]	Residual relative stress level in compression
G_{ft}	[Nm/m^2]	Specific fracture energy in tension
Ω_{tr}	[-]	Residual relative stress level in tension

3.3 Inverse Identification

The actual inverse identification of parameters of the applied material model consisted in repeated computing of the fracture test task for parameter sets generated via a MOGA genetic optimization algorithm within ANSYS Workbench. From each numerical simulation, we exported the data forming the *L-d* curve, and the RMSE factor was employed to facilitate the relevant comparison with the reference curve. The factor was computed in an external application programmed using Python script; the application was called up due to the need of both mapping the numerical *L-d* curves according to the dimension and distributing the reference curve points by means of linear interpolation.

3.3.1 Sensitivity Analysis

The main purpose of the sensitivity analysis is to find out how the output data are influenced by the variability of the input data [23]. This problem can be formulated as an effort to identify the role of specific material parameters in forming the *L-d* curve in the identification of unknown material properties.

The first step of the performed sensitivity analysis was to select the correct output parameter (i.e. the objective function). In accordance with Hyndman *et al*. [24], we chose the Root-Mean-Squared Error (RMSE) measure; this is often used for the calculation of the difference between the values generated by a mathematical model and those that are observed. Such a measure is therefore utilized in meteorology, economics, and demography. The RMSE measure is expressed as follows:

$$\mathrm{RMSE} = \sqrt{\frac{\sum_{1=1}^{n}\left(y_i^{*} - y_1\right)^2}{n}} \tag{1}$$

where y_i^* is the value of the force calculated within the framework of the numerical simulation, and y_i denotes the value of the force gained from the experimental *L-d* curve. However, the direct calculation of the RMSE measure value was complicated by different positions of the points of the numerical and experimental *L-d* curves; this difference had been caused by bisections that occurred during nonlinear solution. It was then necessary to map the points of the numerical *L-d* curve according to the points of the experimental curve, and this process was performed via linear interpolation.

The sought sensitivity was expressed by calculating the Spearman rank-order coefficient of correlation r_s. This statistical measure assesses how well the relationship between two variables can be described using a monotonic function. The calculation of the correlation coefficient was conducted through the use of the programmed Python script. Given that the material parameters and the RMSE measure are real numbers, the value of the Spearman correlation coefficient was calculated using the formula

$$r_s = 1 - \frac{6\sum_{i=1}^{n} \delta_i^2}{n\left(n^2 - 1\right)}, \tag{2}$$

where

$$\delta_i = \mathrm{rank}\left(X_i\right) - \mathrm{rank}\left(Y_i\right) \tag{3}$$

is the difference between the ranks of each observation, and n denotes the number of observations. The sensitivity analysis was performed for 250 samples, while the uniform coverage of the design space was carried out with the LHS method. Due to the importance of both the correct formulation of the objective function for the performance of the sensitivity analysis and the inverse identification based on the optimization algorithm, three different scripts were developed to calculate the RMSE measure on specific parts of the curves.

The first version of the Python script calculated the RMSE sensitivity assumed for the whole length of the *L-d* curves. It was expected that this calculation might not be sufficient, because different parameters participate in the formation of the ascending and descending branches of the *L-d* diagram. On the above-mentioned assumption, the second version of the Python script was developed; thus, the second script calculated two sets of correlation coefficients for two parts of the original *L-d* curve, with splitting at the maximum load point. The idea of splitting the original *L-d* curves into ascending and descending branches led to the development of the third version of the Python script, where the original curves were split into five parts by four specified points. These points might be either chosen by a specific rule or uniformly distributed; in the described task, we selected the latter option. The purpose of developing the third script consisted in the assumption that some parameters may have an influence on specific parts of the curve.

3.3.1 Results of Sensitivity Analysis

The first analysis that calculated the correlation coefficient over the whole length of the *L-d* diagrams showed a higher positive sensitivity (more than 10%) of three material parameters: Young's modulus of elasticity E (r_s = 24.4 %); ultimate tensile strength f_t (r_s = 32.6 %); and specific fracture energy in tension G_{ft} (r_s = 88.6 %). The results of the sensitivity analysis with one objective function are indicated in Fig. 3.

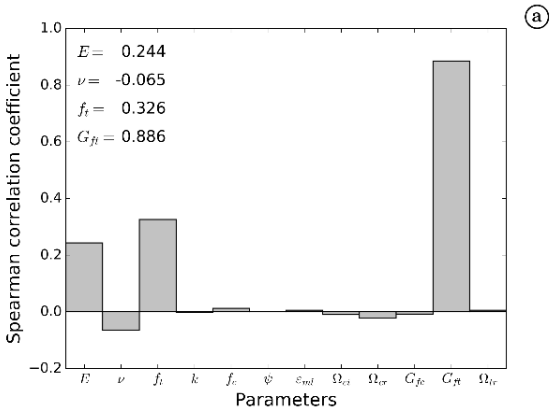

Fig. 3. A sensitivity bar chart – the single RMSE measure

With regard to the fact that the solved task was a three-point bending test, these results were correct but did not eliminate the question of whether some other material parameters had influenced the form of the *L-d* diagram; importantly, such parameters might have been undetected due to a single objective function being used for the whole length of the *L-d* diagram. The second sensitivity analysis was thus performed for two objective functions representing the difference between the ascending and descending branches of the *L-d* diagrams. The graphical appearance of the results of the second sensitivity analysis is shown in Fig. 4 and Fig. 5.

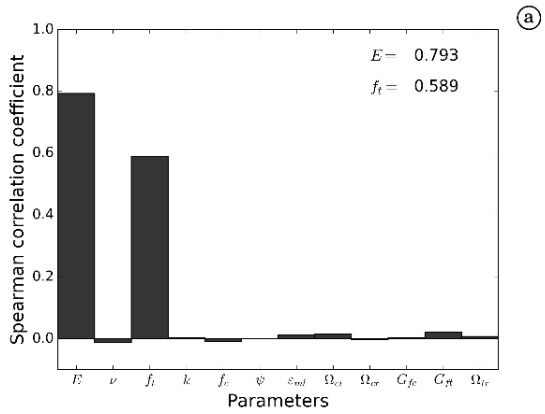

Fig. 4. A sensitivity bar chart – the RMSE measure for the ascending branch

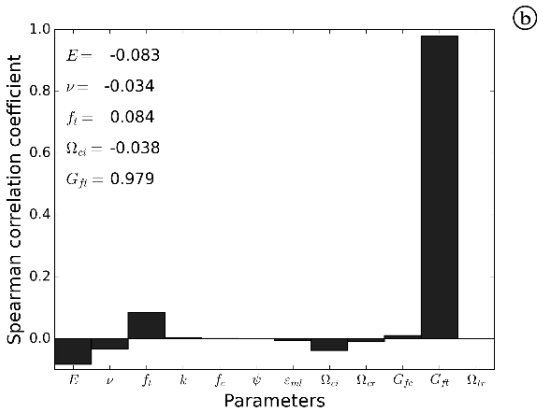

Fig. 5. A sensitivity bar chart – the RMSE measure for the descending branch.

The outcome of the second analysis confirmed the results of the previous one, and it also showed which parts of the *L-d* diagram are influenced by the most significant parameters. The value of the correlation coefficient of Young's modulus of elasticity *E* corresponded to r_s = 79.3%, and this number was higher than that of the correlation coefficient of the ultimate tensile strength, namely, r_s = 58.9%. These results are different in contrast to those obtained from the first sensitivity analysis. A significant influence of just the specific fracture energy with the value of r_s = 97.9% was detected in the descending part of the *L-d* diagram. In fact, the above results did not show the influence of another parameter, and thus the third sensitivity analysis was performed.

The goal of the third analysis was to spread the idea of the previous solution and, mainly, to detect the effect of material parameters in more parts of the *L-d* diagram. The *L-d* diagram was split in five parts so that the first two parts belonged to the ascending branch of the diagram and the last three ones associated with the descending branch. The results of this analysis are presented in Figs. 6 – 10.

The significance of Young's modulus *E* and the ultimate tensile strength f_t in the ascending branch was again confirmed, but, as indicated in Fig. 6 and Fig. 7., the correlation coefficient r_s of the modulus of elasticity of the value r_s = 96.8% was higher in the first part of the diagram. This outcome is a consequence of the linear behavior of the tested specimen at the start of the loading. Interesting results were achieved in the two last parts, where the negative correlation coefficients of the modulus elasticity *E* and the ultimate tensile strength f_t were detected. Such results arose from the substance of the specific fracture energy G_{ft}, which can be described as the area below the *L-d* diagram of simple tensile loading. Here, an increase of the tensile strength and elastic modulus values causes an increase of the RMSE measure value; this effect then leads to a decrease of the specific fracture energy G_{ft} value and vice versa.

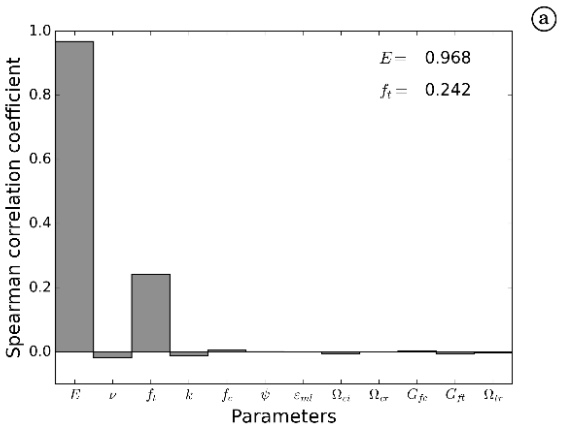

Fig. 6. A sensitivity bar chart – the RMSE measure for the 1st part

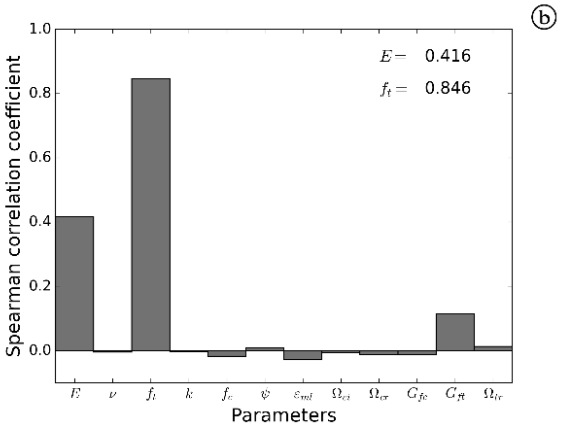

Fig. 7. A sensitivity bar chart – the RMSE measure for the 2nd part

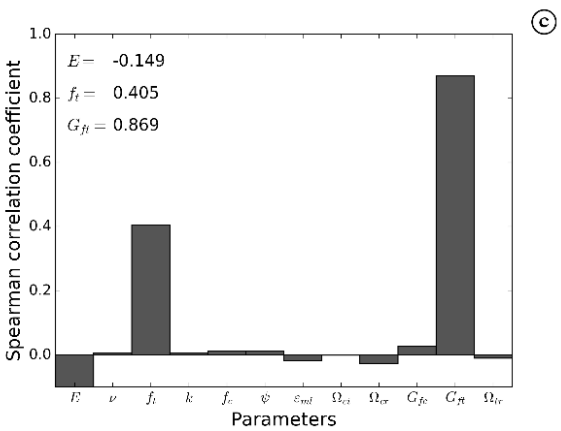

Fig. 8. A sensitivity bar chart – the RMSE measure for the 3rd part

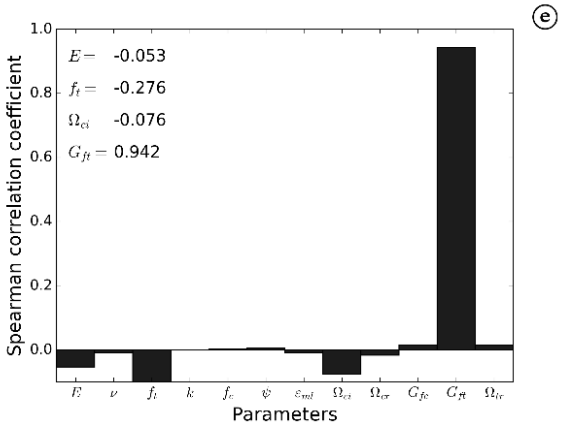

Fig. 9. A sensitivity bar chart – the RMSE measure for the 4th part

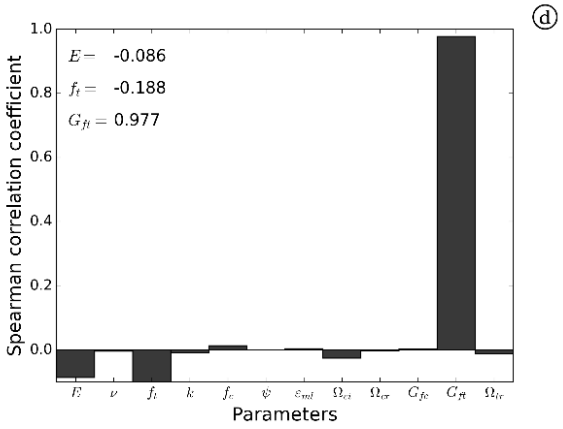

Fig. 10. A sensitivity bar chart – the RMSE measure for the 5th part.

3.3.2 Optimization

As is obvious from the above discussion, the inverse identification was solved as an optimization task aimed to minimize the mutual differences between the reference and the numerically established *L-d* curves, namely, to minimize the RMSE factor. The prescription for the computation of the value thus simultaneously constituted one of the objective function Eq. (1).

Alongside the objective function, we also prescribed inequality conditions in the form:

$$\arctan\frac{f_t}{\sqrt{2}\,f_c} < \psi < \arctan\frac{1}{\sqrt{2}} \tag{4}$$

$$\frac{f_c}{E} < \varepsilon_{ml} \tag{5}$$

Considering a potential lack of convergence between the solutions of certain sets of material parameters, we chose a robust MOGA genetic algorithm to carry out the optimization. The design vector entering into the optimization procedure assumed the shape

$$X = \left\{E, \nu, f_c, f_t, k, \varepsilon_{ml}, \psi, \Omega_{ci}, \Omega_{cr}, G_{fc}, \Omega_{tr}, G_{ft}\right\}^T \tag{6}$$

In the optimization cycle, the execution of 40 design vector generations was preset, with ten individuals in each generation. The resulting optimum, exhibiting the lowest RMSE factor value, was achieved in the 346th execution. By extension, the relevant curves are compared in relation to the identified parameters, Fig. 11; the diagrams indicate good agreement, and the retrieved values can be regarded as the mechanico-physical and fracture-mechanical characteristics of the analyzed material.

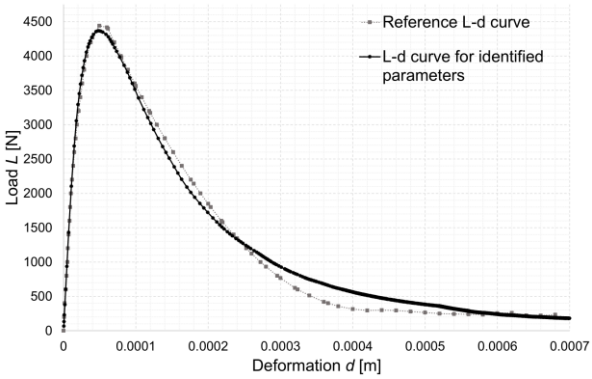

Fig. 11. Comparison of L-d curves

The values of the material model parameters, including the objective function value, are presented in Table 2.

Table 2. Identified material parameters

Par.	Unit	Value
E	[Pa]	$41.843\cdot10^9$
ν	[-]	0.216
f_c	[Pa]	$48.734\cdot10^6$
f_t	[Pa]	$2.323\cdot10^6$
k	[-]	1.245
ψ	[°]	8.953
ε_{ml}	[-]	0.0019
G_{fc}	[Nm/m^2]	0.754
Ω_{ci}	[-]	0.138
Ω_{cr}	[-]	1044.837
G_{ft}	[Nm/m^2]	47.002
Ω_{tr}	[-]	$0.578\cdot10^{-2}$

4 Computing the Load-Carrying Capacity of a Reinforced Concrete Beam

Similarly to the simulation of the fracture experiment, the loading capacity of the applied reinforced concrete window lintel was computed with the finite element method in ANSYS 15.0. To characterize the nonlinear behaviour and to ensure more realistic prediction of the loading capacity of the examined structure, we used the Menétrey-Willam nonlinear model with identified material parameters. Considering the weight of the examined body, which markedly exceeded that of the sample subjected to the fracture experiment, the variants assuming the effect of the object's own weight were solved too; thus, we performed two nonlinear numerical simulations in total.

4.1 Computational Model of a Reinforced Concrete Structure

The computational model of the analyzed window lintel was more comprehensive than that of the examined notched beam, in which it became desirable to reduce the time required for the actual computation. The geometry of the model, within the dimensions shown in Fig. 2, was covered with a mesh of spatial finite elements (SOLID185); each node of these solid, eight-node finite elements comprises 3 translational degrees of freedom. With respect to the anticipated size of the aggregate grains, the edge dimension in each of the elements was set to 5 mm.

Within the computational model, the reinforcement was idealized via LINK180 truss elements, which embody simple, binodal finite elements having three degrees of freedom in each node. This approach appeared to be more advantageous compared to the option based on BEAM188 bar-shaped elements because these need to be secured against rotation due to a higher node valence. The material model of the reinforcement was, considering the nonlinear character of the material model of concrete, set to be elasto-plastic, with a constant plastic branch and kinematic strengthening. The yield value was defined as 500 MPa.

At the location of the supports and load (Fig. 2), we prescribed relevant deformation boundary conditions. Due to the eliminated motion of the body as a rigid unit, horizontal shift was prevented at the load introduction point. The propping in the transverse direction and the prevention of any possible rotation of the entire body were secured where the supports are positioned.

4.1 Numerical Solution

The numerical solution of all the versions was, with respect to the spatial solid elements applied, performed with the PCG (pre-conditioned conjugate gradient) solver; the obtained loading curves are presented in Fig. 12 below.

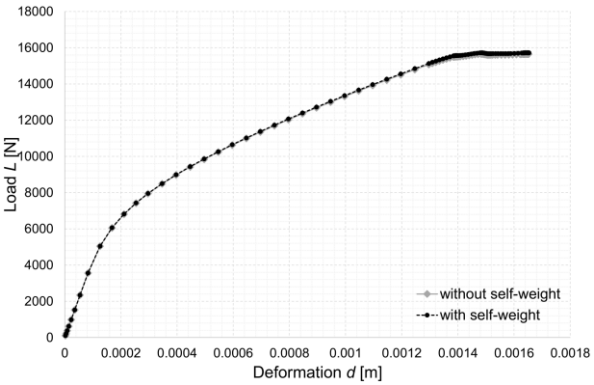

Fig. 12. The resulting L-d curves of the examined reinforced concrete element.

The above-shown diagrams clearly indicate the loading capacity limit of the reinforced concrete element. The value of the loading capacity, or the maximal force, exhibited the magnitudes of $L_{max,num}$ = 15653.1 N in the version neglecting the effect of the self-weight and $L_{max,num,g0}$ = 15721.0 N in the variant considering such impact. The relevant chart exposes strongly nonlinear behaviour of the loaded reinforced concrete element. Within the diagram, it is possible to identify three basic types of behaviour, and these can be outlined as follows: Initially, the element behaved in a linearly elastic manner, and the gradual formation of a crack was accompanied by softening. After the crack has formed, the tensile load in the lower fibers was transmitted only through the concreting reinforcement, which was nevertheless locked in the elastic condition. The ultimate stage then comprised the crushing of the concrete in the compressed section and the transition of the reinforcement from the elastic to the plastic condition.

5 Conclusion

The paper discusses a procedure to determine the loading capacity limits in a reinforced concrete element via numerical simulation, using a nonlinear material model for concrete and reinforcement. The unknown input parameters of the selected material model were found through an inverse analysis exploiting the *L-d* curve measured in the fracture experiment. Within the inverse identification, we

employed a genetic algorithm to identify the parameters summarized in Table 2. One of the possible problems related to the applied identification procedure appears to consist in the fact that all the material parameters were established by means of a test inducing tensile bending stress in the given body; some of the parameters, such as the compression strength or fracture energy, could be identified more suitably with another type of experiment.

The results of the analysis showed us the values of load-carrying capacity of the given reinforced beam and it will be used for comparison with experimental measurements. The shown process of the design of concrete structures with utilization of experimental research and advanced simulation techniques can be considered as bringing the design methods nearer to the real actions of structures.

The most important scientific contribution of the paper is based on utilization of the simple experimental data for simulation of the more complicated structure. It is now possible to use complex material models with large amount of parameters that are not known in advance and predict the behavior of the structures beyond of the elastic limit and thus we are able to design safer and more economically effective structures. The used method is new because of the use of improved sensitivity analysis which can serve not only as the tool for minimizing of the size of the design vector but also as the tool for better understanding of the material model. This feature is derived from the use of more objective functions that are defined on specified parts of the *L-d* curves.

Acknowledgement

The research presented within this paper was supported from the Brno University of Technology project No. FAST-S-16-3718 titled Advanced Numerical Methods with Complex Material Models established to facilitate specialized, university-based research.

References:

[1] Z. Kala, Influence of partial safety factors on design reliability of steel structures - Probability and fuzzy probability assessments, *Journal of Civil Engineering and Management*, Vol. 13, No. 4, 2007, pp. 291–296.

[2] EN 1992-1-1 Eurocode 2: Design of concrete structures – Part 1-1: General rules and rules for buildings, European Committee for Standardization, Brussels, 2004.

[3] T. L. Anderson. *Fracture Mechanics: Fundamentals and applications*. Third edition. Boca Raton: CRC Press, 2004. ISBN 9780849316562.

[4] U. Cicekli, G. Voyiadjis, R. Abu Al-Rub, A plasticity and anisotropic damage model for plain concrete: the origin, evolution, and impact of doi moi, *International Journal of Plasticity*, Vol. 23, No. 10-11, 2007, pp. 1874-1900.

[5] P. Grassl, M. Jirásek, Damage-plastic model for concrete failure. *International Journal of Solids and Structures*. Vol. 43, No. 22-23, 2006, pp. 7166-7196.

[6] J. Ghaboussi, R. Barbosa. Three dimensional discrete element method for granular materials, *International Journal for Numerical and Analytical Methods in Geomechanics*. Vol. 14, 1990, pp. 451–472.

[7] Hušek, M., Kala, J., Hokeš, F., Král, P., How to Handle Irregular Distribution of SPH Particles in Dynamic Fracture Analysis, *International Journal of Theoretical and Applied Mechanics*, Vol. 1, 2016, pp. 212-217, ISSN 2367-8984, 2016.

[8] Kala, J., Hušek, M., Improved Element Erosion Function for Concrete-like Materials with the SPH Method, *Shock and Vibration*, Vol. 2016, 2016, ISSN 1070-9622, 2016

[9] Kala, J., Hušek, M., High speed loading of concrete constructions with transformation of eroded mass into the SPH, *International Journal of Mechanics*, Vol. 10, 2016, pp. 145-150, ISSN 1998-4448, 2016

[10] T. Belytschko, T. Black, Elastic crack growth in finite elements with minimal remeshing, *International Journal for Numerical Methods in Engineering*. Vol. 45, No. 5, 1999, pp. 601–620.

[11] DYNARDO, GmbH. *Multiplas: User's Manual Release 5.1.0 for 15.0*. Weimar, 2014.

[12] ANSYS, Inc. *Release 15.0 Documentation for ANSYS*. Southpointe 275 Technology Drive Canonsburg, PA 15317, 2012.

[13] P. Král, J. Kala, and P. Hradil, Verification of the Elasto-Plastic Behavior of Nonlinear Concrete Material Models, *International Journal of Mechanics*, vol. 10, pp. 175-181, 2016, ISSN: 1998-4448.

[14] D. Novák, D. Lehký, ANN inverse analysis based on stochastic small-sample training set simulation, *Engineering Applications of Artificial Intelligence*, Vol. 19, No. 7, 2006, pp. 731-740.

[15] F. Hokes, J. Kala, O. Krnavek, Nonlinear numerical simulation of fracture test with use of optimization for identification of material parameters, *International Journal of Mechanics*, Vol. 10, 2016, pp. 159-166. ISSN 1998-4448 138.

[16] F. Hokeš, J. Kala, M. Hušek, P. Král, Parameter Identification for a Multivariable Nonlinear Constitutive Model inside ANSYS Workbench, *Procedia Engineering*, Vol. 161, 2016, pp. 892-897, ISSN 1877-7058, http://dx.doi.org/10.1016/j.proeng.2016.08.743.

[17] A. Strauss, T. Zimmermann, D. Lehký, D. Novák, Z. Keršner, Stochastic fracture-mechanical parameters for the performance-based design of concrete structures. *Structural Concrete*, Vol. 15, No. 3, 2014 pp. 380-394.

[18] J. C. Simo, T. J. R. Hughes, *Computational inelasticity*. New York: Springer, 1998. ISBN 978-038-7227-634.

[19] P. Menétrey, *Numerical analysis of punching failure in reinforced concrete structures*. Lausane. PhD Thesis, EPFL, 1994.

[20] K. J. Willam, E. P. Warnke, E. P. Constitutive model for the triaxial behavior of concrete, *International Association of Bridge and Structural Engineers*, Vol. 19, 1974, pp. 1-30.

[21] R. Pölling, *Eine praxisnahe, schädigungsorienten Materialbeschreibung von Stahlbeton für Strukturanalysen*. Bochum. PhD Thesis, Ruhr-Universität, 2000.

[22] Z. P. Bažant, B. H. Oh, Crack band theory for fracture of concrete, *Matériaux et Constructions*, Vol. 16, No. 3, 1983, pp. 155-177, 1983.

[23] Z. Kala, J. Kala, M. Škaloud, and B. Teplý, Sensitivity analysis of the effect of initial imperfections on the (i) ultimate load and (ii) fatigue behaviour of steel plate girders, *Journal of Civil Engineering and Management*, Vol. 11, No. 2, 2005, pp. 99–107.

[24] R. J. Hyndman, A. B. Koehler, Another look at measures of forecast accuracy, *International Journal of Forecasting*, Vol. 22, No. 4, 2006, pp. 679-688.